Research Article

Microstructures and Toughening of TiC-TiB$_2$ Ceramic Composites with Cr-Based Alloy Phase Prepared by Combustion Synthesis in High-Gravity Field

Xuegang Huang,[1,2] **Chun Yin,**[3] **Zhongmin Zhao,**[1] **Long Zhang,**[1] **and Junyan Wu**[1]

[1]*Department of Vehicle and Electrical Engineering, Mechanical Engineering College, Shijiazhuang 050003, China*
[2]*China Aerodynamics Research & Development Center, Mianyang 621000, China*
[3]*School of Automation Engineering, University of Electronic Science and Technology of China, Chengdu 611731, China*

Correspondence should be addressed to Xuegang Huang; emei-126@126.com

Micro-nanocrystalline microstructures which are characterized by TiB$_2$ platelets of the average thickness close to or smaller than $1\,\mu$m can be achieved in nearly full-density solidified TiC-TiB$_2$ ceramic composites with Cr-based alloy phases by combustion synthesis in ultra-high gravity field of 2500 g. The filler phases in ceramic composites are actually Cr-based alloy with a little solidified solution of Ni atoms and Al atoms. The hardness, flexural strength, and fracture toughness of the materials are 18.5 ± 1.5 GPa, 650 ± 35 MPa, and 16.5 ± 1.5 MPa·m$^{0.5}$, respectively. The improved fracture toughness of TiC-TiB$_2$ ceramic composites results from crack deflection, crack bridging, and pull-out by a large number of fine TiB$_2$ platelets and plastic deformation with some Cr-based alloy phases.

1. Introduction

TiC and TiB$_2$ have become the promising candidates for cutting tools, wear-resistant parts, forming dies, and light-weight amour pieces, because of the many desirable properties they possess, such as high hardness, low density, high melting temperature, high corrosion resistance, good thermal shock resistance, and high temperature stability [1]. Meanwhile, the TiC-TiB$_2$ composites exhibit excellent high-temperature performance which makes them also desirable for aircraft propulsion systems and thermal protection systems of space vehicle and nuclear fusion reactor. Therefore, in recent years many methods have been developed to prepare full-density TiC-TiB$_2$ composites, such as high-pressure sintering (HPS) with or without sintering aids, reactive sintering (RS), reaction hot pressing (RHP), pressureless sintering (PS), spark plasma sintering (SPS), transient plastic phase processing (TPPP), self-propagating high-temperature synthesis (SHS), and combustion synthesis (CS) [2–5].

However, based on the achievements in preparing TiC-TiB$_2$ composites, Vallauri et al. [2] concluded that the microstructures of bulk TiC-TiB$_2$ composites were rarely characterized by the size of crystal grains close to or smaller than $1\,\mu$m, making the flexural strength of TiC-TiB$_2$ composites hardly exceed 800 MPa [6]. Moreover, the known toughening mechanisms of the ceramics, such as transformation toughening and fiber toughening, are difficult to employ in TiC-TiB$_2$ composites because of the extremely high sintering temperature which results in the fracture toughness of the materials generally smaller than 7.0 MPa·m$^{0.5}$ [2]. Therefore, to promote the strengthening and toughening of hard materials, new approaches have always been sought and tried out to prepare bulk TiC-TiB$_2$ composites with ultrafine-grained microstructures that possess intensive toughening mechanisms [7].

Combustion synthesis is being used to produce ceramics, intermetallics, and composite materials [8, 9]. Therefore, a new method, named combustion synthesis under high gravity, has been worked out to prepare high-hardness ceramic or cermets composites. This new approach has the advantages of high efficiency, low energy cost, simple equipment, and easy centrifugal forming [10–13]. The paper will illustrate

TABLE 1: Composition of the ceramic composites in the corresponding region of Figure 2 (atomic, %).

| Position	Ti	C	B	Cr	Ni	Al	Determined phase
1	33.88	—	60.91	1.08	1.16	2.97	TiB$_2$
2	49.02	40.79	—	4.46	2.46	3.27	TiC
3	2.78	—	—	69.10	15.11	13.01	Cr-based alloy

the experiment renewed by adjusting the components of the combustion system to control the composition of solidified TiC-TiB$_2$ ceramic, which contributes to the ultrafine-grained microstructures of the materials. What is more, the paper will also expand on the microstructures and mechanical properties as well as the strengthening and toughening mechanisms of the solidified TiC-TiB$_2$ ceramics with Cr-based alloy.

2. Experimental

Commercial powders of Ti (99.5% purity, <34 μm), B$_4$C (97% purity, <3 μm), CrO$_3$ (99.9% purity, <60 μm), Al (96% purity, <50 μm), and Ni (99.85% purity, <10 μm) were used as raw materials. The molar ratio (Ti to B$_4$C) of 3 : 1 was chosen as the starting composition, so the composition of the solidified TiC-TiB$_2$ composite was determined as TiC-66.7 mol % TiB$_2$. According to previous research results [14–16], due to the lower melting temperature and good wettability of Ni to TiC-TiB$_2$, the introduction of Ni into combustion system could enhance the flowability and dwell time of ceramic liquid products, which will help to improve the density and homogeneity of ceramic products as a result of the forced convection and filling at the final stage of the solidification process. Based on the reason mentioned above, about 5 wt% Ni additive agent was introduced into the Ti + B$_4$C combustion system, as shown in (1). In order to ensure high-temperature and full-liquid products after the combustion reaction, a 25 wt% (CrO$_3$ + Al) subsystem was added as the activator to increase the combustion temperature, as shown in (2). Consider

$$3Ti + B_4C + xNi \longrightarrow TiC + 2TiB_2 + xNi \quad (1)$$

$$CrO_3 + 2Al \longrightarrow Al_2O_3 + Cr \quad (2)$$
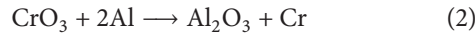
The above powder blends were mechanically homogenized by ball milling for 1 h. After that, the graphite crucibles were filled with the reactive mixtures (1 kg) under uniaxially cold-press about 200 MPa. Then the graphite crucibles were inserted into the combustion chambers at the end of the rotating arms of the centrifugal machine. The combustion reaction was triggered by the electrical heat W wire (diameter of 0.5 mm) while the centrifugal machine provided a high-gravity acceleration of 2500g (g = 9.8 m/s^2, where g means the gravitational constant). When the combustion reaction was over, the centrifugal machine continued to run for 30 seconds. When the crucibles were cooled to ambient temperature, the ceramic discs of 150 mm in diameter and 15 mm in thickness were obtained after the samples were taken out of the graphite crucibles and the oxide slag at the top of the sample was eliminated by grinding.
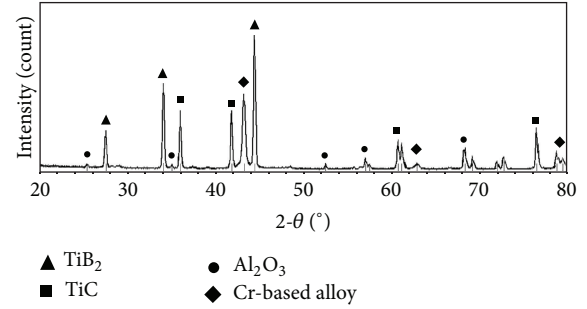
FIGURE 1: The XRD pattern of the TiC-TiB$_2$ ceramic composites.

The ceramic discs were cut and ground into rectangular bars measuring 3 mm (width) × 4 mm (height) × 36 mm (length) to determine their flexural strength. The flexural strength was measured by the three-point bending method with a cross-head speed of 0.5 mm·min^{-1} and a span of 30 mm. The indentation test was conducted with a loading time of 15 s and a load scale of 196 N to determine the hardness and fracture toughness of the ceramic composites. The phase composition was identified by X-ray diffraction (XRD; D/max-PA, Rigaku, Japan) with a step of 0.02° and a scanning rate of 2°/min. The microstructure and fracture morphology were examined by field emission scanning electron microscopy (FESEM; JSM-7001F, JEOL, Japan). The electron probe microanalysis (EPMA) was conducted by energy dispersive spectrometry (EDS).

3. Results and Discussion

The XRD spectra of the samples showed that the ceramics were mainly composed of the phases of TiC and TiB$_2$. In addition, a few inclusions of α-Al$_2$O$_3$ and a minute amount of Cr-based alloy were also detected (as shown in Figure 1). The diffraction crystal planes of TiC were (111), (200), and (220), while the diffraction crystal planes of TiB$_2$ were (001), (100), (101), and (002). The maximum diffraction-intensity crystal planes of TiC and TiB$_2$ were (200) and (101), respectively. Because of the mole percent of Ni atoms which is much less than that of Cr atoms as well as the intersolubility of Cr and Ni at high temperature, the diffraction patterns of Cr but not Ni were detected by XRD in this experiment.

FESEM images and EDS spectra showed that a large number of randomly orientated, fine TiB$_2$ platelets (presented by the dark areas in Figure 2) were uniformly embedded in irregular TiC grains (presented by the grey areas in Figure 2) and Cr-based alloy (presented by the white areas in Figure 2). Besides, a few inclusions of α-Al$_2$O$_3$ were also observed, as shown by the isolated black particles in Figure 2. For the white Cr-based alloy, some Ni atoms and residual Al atoms were detected by EDS results in Table 1, and the atomic ratio of Cr,
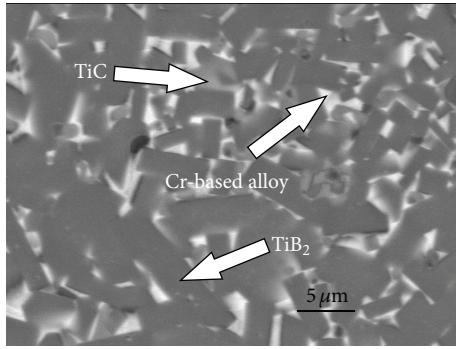
FIGURE 2: FESEM microstructure of the TiC-TiB$_2$ ceramic composites.

FIGURE 3: FESEM microstructure of TiC-TiB$_2$ ceramic surface.

Ni, Al was about $69:15:13$. Consequently, it can be concluded that the alloy was actually the Cr-based alloy phase with a little solid solution of Ni atoms and residual Al atoms. CrO$_3$ powder is a strong oxidant of the thermit, which is chemically unstable because of its decomposition at low temperature of 170°C [17]; the ignition of CrO$_3$-Al mixture can occur at low temperature due to the presence of free oxygen atoms, as shown in (3). Judging from (2) and (3), the addition amount of Al powder to the combustion system is sufficient to support the thermit reaction, whereas the residual Al atoms have to be reserved in Cr-Ni liquid alloy, which in turn leads to the formation of the Cr-based alloy among the hard phases of TiC and TiB$_2$ at the final stage of solidification, as shown in Figure 2:

$$2CrO_3 \longrightarrow Cr_2O_3 + 3O \qquad (3)$$
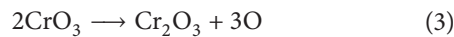
The FESEM images showed that the refinement of TiB$_2$ platelets was observed to arise from the centre to the surface of the sample, and the average thickness of TiB$_2$ platelets decreased from about $2\,\mu m$ at the center to $1\,\mu m$ on the surface, whereas the average aspect ratio of TiB$_2$ platelets changed from 5.25 to 2.38 inversely, as shown in Figures 2 and 3. White Cr-based alloy phases were rarely observed on the surface of the ceramic. Therefore, it can be concluded that the unique micro-nanocrystalline microstructure and the change in geometrical size of TiB$_2$ platelets are closely dependent on the solidification behavior of the materials and the crystal growth of TiB$_2$ and TiC.

Since the composition of the current TiC-TiB$_2$ composites is chosen as TiC-66.7 mol% TiB$_2$ of the hypereutectic composites based on some reports [18, 19], TiB$_2$, in fact, acts as the primary phase to nucleate and precipitate from the melt. However, the TiC-TiB$_2$ composite is achieved by rapid solidification, so crystal growth and crystal morphology of TiB$_2$ are mainly controlled by the attachment energy of crystal plane to the atoms of Ti and B [20]. According to the atom-bonding strength of TiB$_2$ lattice, that is, B–B > Ti–B > Ti–Ti, the growth velocities of crystal planes in TiB$_2$ can be determined as $(0001) < (10\bar{1}0) < (10\bar{1}1) < (1\bar{2}10) < (1\bar{2}11)$ [21]. In other words, the crystallographic characteristics of TiB$_2$ lattice lead to the anisotropy in crystal growth of TiB$_2$, making TiB$_2$ grow at the preferred crystal plane of high
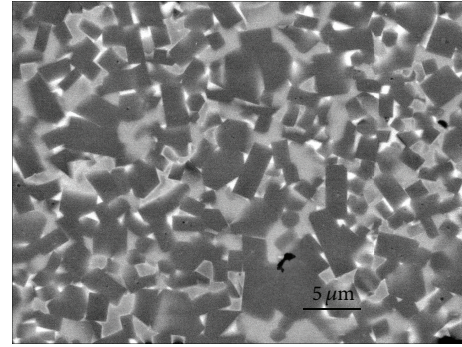
indices, such as $(1\bar{2}10)$ and $(1\bar{2}11)$. Accordingly, as TiB$_2$ crystal is in contact with TiC and other TiB$_2$ crystals, or the high-indices planes of TiB$_2$ crystal cannot capture enough Ti and B atoms to support its growth, the growth at high-indices planes of TiB$_2$ crystal comes to a stop. However, the low-indices planes of TiB$_2$ crystal continue to grow until the TiB$_2$ crystal is enveloped by its low-indices crystal planes of $(10\bar{1}0)$ and $(10\bar{1}1)$, and the TiB$_2$ platelet with finite aspect ratio is developed while the low-indices crystal planes of (101) and (001) become the first-intensity and second-intensity diffraction planes of TiB$_2$ phases, as illustrated in XRD spectra. Thereby, low-velocity faceting growth of TiB$_2$ solid is one of the reasons for the achievement of fine TiB$_2$ platelets and ultrafine-grained microstructures of the ceramic. With the continuous precipitation of TiB$_2$ crystals out of the melt, TiC crystals also begin to precipitate as the concentration of C atoms in the melt becomes greater than the mole concentration of C which is indispensable to the nucleation of TiC crystal. Because TiC is characterized by a B1 (or NaCl-type) crystal structure with the isotropy in crystallography, it has a strong tendency of high-velocity nonfaceting growth. Therefore, under the dual influence of growth characteristics of TiC crystal and high diffusion rate of C relative to B [2], TiC grows much faster than TiB$_2$ does once TiC is nucleated. Thus, the rapid growth of TiC not only contests against TiB$_2$ for more Ti atoms, but also competes against TiB$_2$ for more growing space, making it more difficult for TiB$_2$ to be coarsened; then, a majority of TiB$_2$ platelets are rapidly surrounded by irregular TiC grains. Therefore, the rapid growth of TiC second phase is another reason for the achievement of ultrafine-grained microstructures in current TiC-TiB$_2$ composites.

In addition, crystal growth of TiB$_2$ is also controlled by the solidification conditions, involving temperature gradient and heat dissipation of the melt. At the initial stage of solidification, high nucleation rate and low growth velocity of TiB$_2$ crystals arise near the inner wall of the crucible due to high temperature gradient and fast heat dissipation. However, with the development of the heat-insulation ceramic solidifying toward the centre, heat dissipation and temperature gradient of the melt decrease while thermal diffusion in the melt increases inversely. Thus, the microstructure gradually transforms from nanocrystalline to microcrystalline, which
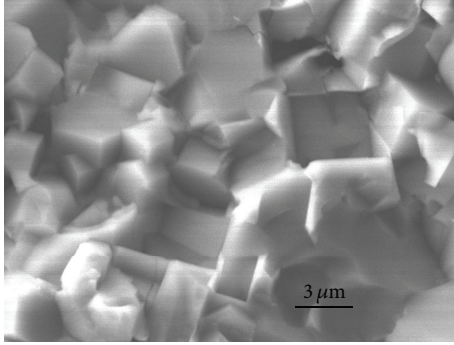
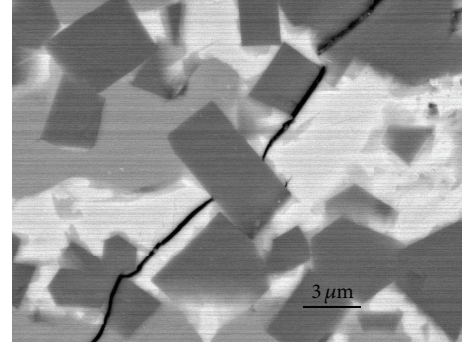FIGURE 4: FESEM fracture morphology of TiC-TiB$_2$ ceramic composites.

FIGURE 5: FESEM image of crack propagation paths in TiC-TiB$_2$ ceramic composites.

can be illustrated by the increase in the average thickness of TiB$_2$ platelets and the decrease in their average aspect ratio. The change in solidification behavior of the ceramic is also the reason for the concentration of Cr-Ni-Al alloy phases at the centre of the sample.

The relative density of TiC-TiB$_2$ achieved measured 99.5%. The characteristics of combustion reaction in high-gravity field are similar to thermal explosives, which not only help the gas escape rapidly, but also form the thermal vacuum around liquid products. The achievement of the full-density ceramic derives both from the rapid solidification of the ceramic in high-gravity field and, more importantly, from the presence of Cr-Ni-Al alloy as the final solidified phase to eliminate shrinkage cavities. The hardness, flexural strength, and fracture toughness of the current solidified TiC-TiB$_2$ measured 18.5 ± 1.5 GPa, 650 ± 35 MPa, and 16.5 ± 1.2 MPa·m$^{0.5}$. Compared with the maximum hardness of 28.5 GPa [14], the maximum flexural strength of 800 ± 30 MPa [14], and the maximum fracture toughness of 12.20 ± 1.26 MPa·m$^{0.5}$ [22] reported by the literature, the current TiC-TiB$_2$ composite has higher fracture toughness, yet, its hardness is only moderate. It is worthy to note that despite the general moderate hardness measured in current composites, the maximum hardness of 20.0 ± 2.0 GPa was achieved on the surface, while the minimum hardness of 17.5 ± 1.0 GPa was achieved in the center of the ceramic. Therefore, the presence of Cr-Ni-Al alloy phases is the very reason for the average hardness of the current composite, smaller than one of the materials prepared by early experiments.

FESEM fracture morphologies showed that the fracture behavior of TiC-TiB$_2$ composite ceramics presented a mixed mode of transgranular fracture in TiC irregular grains and intercrystalline fracture along TiB$_2$ platelets, and the grooves of TiB$_2$ platelets clearly remained at fracture section of the ceramic after they were peeled out of the ceramic matrix, as shown in Figure 4. Meanwhile, FESEM images of crack propagation paths showed that crack deflection and crack bridging seemed to be the main interaction mechanisms of the crack and TiB$_2$ platelets, as shown in Figure 5.

According to the literature [23], the larger grain size of TiC crystals means the smaller critical shear stress inducing the cracking of TiC grains, so transcrystalline fracture almost takes place in the coarsened irregular TiC grains as shown

in Figure 6(a). At ambient temperature, the cleavage surface and tearing ridge, which were taken as typical brittle transcrystalline fracture features, can be partially seen on fracture surfaces as shown in Figure 6(b). It is also demonstrated that TiC phases have little effect on ceramic toughening, but they do play a role in ceramic strengthening by refining the microstructure of the ceramic during solidification. As for TiB$_2$, in contrast, the crack is firstly arrested and crack-pinning effect is initiated as the crack is met by these small-thickness TiB$_2$ platelets, which results from their high elastic modulus, high volume fraction, plate-like morphology, and highly random distribution, especially their thickness close to or smaller than 1 μm. Subsequently, the crack has to propagate around the TiB$_2$ platelets due to the weak interfacial bonding between TiB$_2$ phases and the other ones, and crack deflection toughening mechanism occurs. With the propagation of the crack and the debonding at the interfaces of TiB$_2$ platelets, secondary microcracks develop along the boundaries of TiB$_2$ phases, resulting in the presence of crack bridging along with frictional interlocking as a result of the growth of secondary microcracks at both sides of the interface. Finally, crack bridging or pull-out of TiB$_2$ platelet is accomplished, as shown in Figure 7. Thus, greater crack-opening displacement within the bridging zone is achieved, whereas the stress concentration around the crack tip is relieved due to the presence of the closure stress behind it, which in turn results in greater resistance to crack propagation in the ceramic. Therefore, it is reasonable to conclude that, by acting as the reinforcement in the ceramic, small-thickness TiB$_2$ platelets play a predominant role in strengthening and toughening the ceramic through their interaction with the crack to induce the toughening mechanisms of crack deflection, crack bridging, or pull-out of the platelet. In addition, the fracture toughness on the surface of the ceramic measures 13.6 ± 1.5 MPa·m$^{0.5}$ by indentation test, whereas the fracture toughness in the central part measures 18.8 ± 2.0 MPa·m$^{0.5}$. Slight yield phenomenon can also be observed in load-displacement curve of the material, so we can come to the conclusion that, besides the toughening mechanisms induced by TiB$_2$ platelets, Cr-Ni-Al alloy phases also play an important role in toughening ceramic through their plastic deformation, as shown in Figure 8. When the crack extends through the Cr-Ni-Al alloy phases and forms the cleavage steps and tear ridges, the
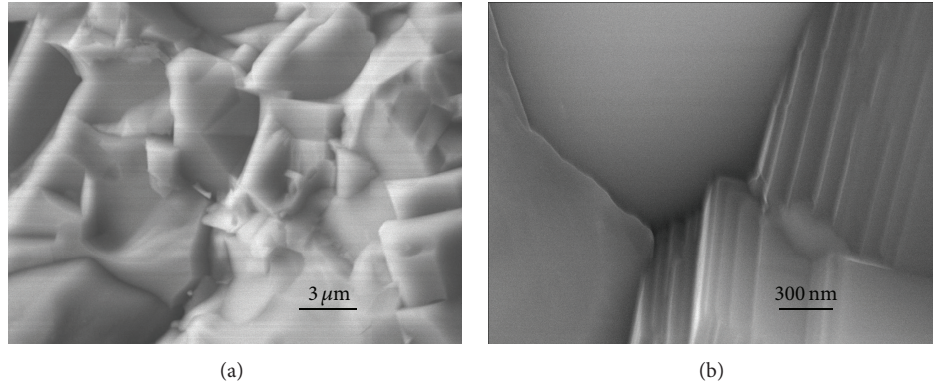
(a)

(b)

FIGURE 6: FESEM fracture morphologies in the coarsened irregular TiC grains: (a) fracture surface in TiC grains, (b) the cleavage surface and tearing ridge.
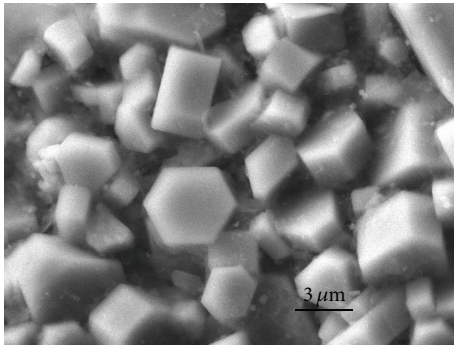

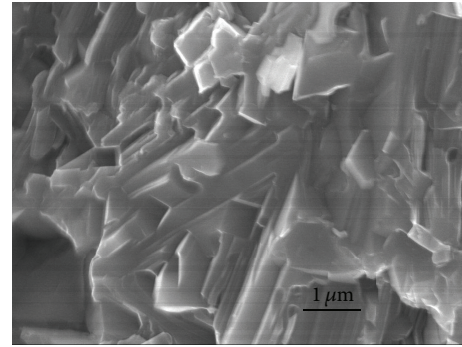FIGURE 7: Fracture surface after crack bridging or pull-out of TiB_2 platelet.

FIGURE 9: Transgranular cleavage patterns in Cr-Ni-Al alloy phases.
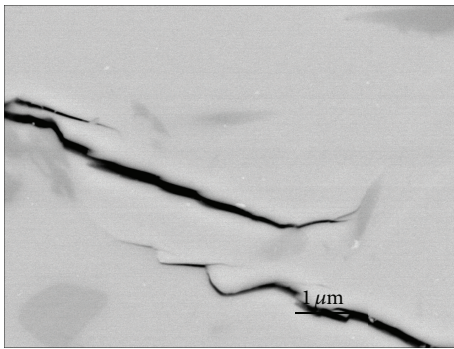

FIGURE 8: FESEM image of crack propagation paths in Cr-Ni-Al alloy phases.

transgranular cleavage fracture is more easily to arise in the Cr-based alloy phases with some aluminum and nickel content, as shown in Figure 9.

Accordingly, by combining the microstructures of the ceramic with linear elastic fracture mechanics for I-mode crack [24], high flexural strength of the current composite is considered to derive from the achievement of full-density ceramic, high volume fraction of high-elastic-modulus TiB_2. Moreover, the achievement of micro-nanocrystalline

microstructure in the full-density ceramic secures high fracture toughness, and the fracture behavior of the ceramic composites is controlled by the intensively coupled mechanisms of crack deflection, crack bridging, or pull-out by a large number of fine TiB_2 platelets, along with the plastic deformation of the Cr-Ni-Al alloy phases.

4. Conclusion

To sum up, TiC-TiB_2 ceramic composites with micro-nanocrystalline microstructures can be achieved by combustion synthesis in high-gravity field. XRD, FESEM, and EDS show that a large number of fine TiB_2 platelets are uniformly embedded in irregular TiC grains, and a few Cr-Ni-Al alloy phases can be detected in or between those phases. The average thickness of TiB_2 platelets decreases from the center to the surface of the materials, whereas their average aspect ratio increases inversely. Cr-Ni-Al alloy phases are also found in the central part of the composite. The achievement of micro-nanocrystalline microstructures, characterized by TiB_2 platelets with the average thickness close to or smaller than $1\,\mu m$ in the ceramic, results from the low-velocity faceting growth of TiB_2 crystal due to its anisotropy in crystallography, the high-velocity nonfaceting growth of TiC solid due to its isotropy in crystallography, and high diffusion rate of B relative to C in liquid TiC-TiB_2. These combine to

make the growth velocity of TiC faster than that of TiB_2, despite the fact that the TiB_2 solid serves as the leading phase at the initial stage of solidification, which hardly renders TiB_2 platelets to grow and coarsen so as to be surrounded rapidly by irregular TiC grains during solidification. The relative density of TiC-TiB_2 composites measures 99.5%, and the achievement of the nearly full-density composites is a result of the rapid solidification of the ceramics in high-gravity field and the presence of a few low-melting-point Cr-based alloys. The hardness, flexural strength, and fracture toughness of solidified TiC-TiB_2 measure $18.5 \pm 1.5\,\mathrm{GPa}$, $650 \pm 35\,\mathrm{MPa}$, and $16.5 \pm 1.2\,\mathrm{MPa \cdot m^{0.5}}$, respectively. High flexural strength of the materials is achieved as a result of the high volume fraction of high-elastic-modulus TiB_2. The high fracture toughness derives from intensively coupled mechanisms of crack deflection, crack bridging, and pull-out by a large number of fine TiB_2 platelets as well as the plastic formation of Cr-Ni-Al alloy phases.

Conflict of Interests

The authors declare that there is no conflict of interests regarding the publication of this paper.

Acknowledgment

References

[1] E. T. Akinlabi, R. M. Mahamood, S. A. Akinlabi, and E. Ogunmuyiwa, "Processing parameters influence on wear resistance behaviour of friction stir processed Al-TiC composites," *Advances in Materials Science and Engineering*, vol. 2014, Article ID 724590, 12 pages, 2014.

[2] D. Vallauri, I. C. Atías Adrián, and A. Chrysanthou, "TiC-TiB$_2$ composites: a review of phase relationships, processing and properties," *Journal of the European Ceramic Society*, vol. 28, no. 8, pp. 1697–1713, 2008.

[3] Y. H. Liang, H. Y. Wang, Y. F. Yang, Y. L. Du, and Q. C. Jiang, "Reaction path of the synthesis of TiC-TiB$_2$ in Cu-Ti-B$_4$C system," *International Journal of Refractory Metals and Hard Materials*, vol. 26, no. 4, pp. 383–388, 2008.

[4] B. Aminikia, "Investigation of the pre-milling effect on synthesis of nanocrystalline TiB$_2$-TiC composite prepared by SHS method," *Powder Technology*, vol. 232, pp. 78–86, 2012.

[5] F. Kustas, B. Mishra, and J. Zhou, "Fabrication and characterization of TiB$_2$/TiC and tungsten co-sputtered wear coatings," *Surface and Coatings Technology*, vol. 153, no. 1, pp. 25–30, 2002.

[6] D. Brodkin, A. Zavaliangos, S. R. Kalidindi, and M. W. Barsoum, "Ambient- and high-temperature properties of titanium carbide-titanium boride composites fabricated by transient plastic phase processing," *Journal of the American Ceramic Society*, vol. 82, no. 3, pp. 665–672, 1999.

[7] Y. F. Yang, H. Y. Wang, R. Y. Zhao, Y. H. Liang, and Q. C. Jiang, "Effect of Ni content on the reaction behaviors of self-propagating high-temperature synthesis in the Ni–Ti–B$_4$C system," *International Journal of Refractory Metals and Hard Materials*, vol. 26, no. 2, pp. 77–83, 2008.

[8] T. K. Barkley, J. E. Vastano, J. R. Applegate, and S. D. Bakrania, "Combustion synthesis of Fe-incorporated SnO$_2$ nanoparticles using organometallic precursor combination," *Advances in Materials Science and Engineering*, vol. 2012, Article ID 685754, 8 pages, 2012.

[9] J. Yu, K. Matsuura, and M. Ohno, "Combustion synthesis of TiC-TiB$_2$-based cermets from elemental powders," *Advances in Tribology*, vol. 2011, Article ID 105258, 8 pages, 2011.

[10] G. Liu and J. Li, "High-gravity combustion synthesis: a fast and furnace-free way for preparing bulk ceramic materials," *Journal of Asian Ceramic Societies*, vol. 1, no. 2, pp. 134–142, 2013.

[11] C. Yin, Y. Chen, and S. M. Zhong, "Fractional-order sliding mode based extremum seeking control of a class of nonlinear systems," *Automatica*, vol. 50, no. 12, pp. 3173–3181, 2014.

[12] C. Yin, S.-m. Zhong, and W.-f. Chen, "Design of sliding mode controller for a class of fractional-order chaotic systems," *Communications in Nonlinear Science and Numerical Simulation*, vol. 17, no. 1, pp. 356–366, 2012.

[13] C. Yin, B. Stark, Y. Q. Chen, S. M. Zhong, and E. Lau, "Fractional-order adaptive minimum energy cognitive lighting control strategy for the hybrid lighting system," *Energy and Buildings*, vol. 87, pp. 176–184, 2015.

[14] X. G. Huang, L. Zhang, Z. M. Zhao, and C. Yin, "Microstructure transformation and mechanical properties of TiC-TiB$_2$ ceramics prepared by combustion synthesis in high gravity field," *Materials Science and Engineering: A*, vol. 553, pp. 105–111, 2012.

[15] X. Huang, Z. Zhao, L. Zhang, and J. Wu, "The effects of ultra-high-gravity field on phase transformation and microstructure evolution of the TiC-TiB$_2$ ceramic fabricated by combustion synthesis," *International Journal of Refractory Metals and Hard Materials*, vol. 43, pp. 1–6, 2014.

[16] R. Mahmoodian, M. A. Hassan, M. Hamdi, R. Yahya, and R. G. Rahbari, "In situ TiC–Fe–Al$_2$O$_3$–TiAl/Ti$_3$Al composite coating processing using centrifugal assisted combustion synthesis," *Composites Part B: Engineering*, vol. 59, pp. 279–284, 2014.

[17] W. J. Lee, Z. A. Munir, and M. Ohyanagi, "Dense nanocrystalline TiB$_2$-TiC composites formed by field activation from high-energy ball milled reactants," *Materials Science and Engineering A*, vol. 325, no. 1-2, pp. 221–227, 2002.

[18] W. J. Li, R. Tu, and T. Goto, "Preparation of directionally solidified TiB$_2$-TiC eutectic composites by a floating zone method," *Materials Letters*, vol. 60, no. 6, pp. 839–843, 2006.

[19] B. Zou, P. Shen, Z. Gao, and Q. Jiang, "Combustion synthesis of TiC$_x$-TiB$_2$ composites with hypoeutectic, eutectic and hypereutectic microstructures," *Journal of the European Ceramic Society*, vol. 28, no. 11, pp. 2275–2279, 2008.

[20] A. A. Abdel-Hamid, S. Hamar-Thibault, and R. Hamar, "Crystal morphology of the compound TiB$_2$," *Journal of Crystal Growth*, vol. 71, no. 3, pp. 744–750, 1985.

[21] W.-J. Li, R. Tu, and T. Goto, "Preparation of directionally solidified TiB$_2$-TiC eutectic composites by a floating zone method," *Materials Letters*, vol. 60, no. 6, pp. 839–843, 2006.

[22] G. Wen, S. B. Li, B. S. Zhang, and Z. X. Guo, "Reaction synthesis of TiB$_2$-TiC composites with enhanced toughness," *Acta Materialia*, vol. 49, no. 8, pp. 1463–1470, 2001.

[23] T. H. Courtney, *Mechanical Behavior of Materials*, McGraw-Hill, New York, NY, USA, 2nd edition, 2000.

[24] J. S. Zhang, *Material Strength*, HIT Press, Harbin, China, 2004.